Substrate-Mediated Growth of Oriented, Vertically Aligned MoS_2 Nanosheets on Vicinal and On-axis SiC Substrates

Jonathan Bradford,[1,2] Aurora Zaganelli,[3] Dongchen Qi,[1,4] Negar Zabardastan,[1] Mahnaz Shafiei,[5,6] Jennifer MacLeod,[1,4,6] and Nunzio Motta[1,4,6,*]

[1]*School of Chemistry and Physics, Queensland University of Technology (QUT), Brisbane, QLD, Australia*

[2] *School of Physics and Astronomy, University of Nottingham, Nottingham NG7 2RD, United Kingdom*

[3] *Dipartmento di Fisica, Universita degli Studi di Roma "Tor Vergata", Rome, Italy*

[4] *Centre for Materials Science, Queensland University of Technology (QUT), Brisbane, QLD, Australia*

[5]*Faculty of Science, Engineering and Technology, Swinburne University of Technology, Hawthorn, VIC, Australia*

[6]*Institute for Future Environments, Queensland University of Technology (QUT), Brisbane, QLD, Australia*

*Corresponding Author: n.motta@qut.edu.au

Abstract

The layer- and morphology-dependent properties of two-dimensional molybdenum disulfide (MoS_2) have established its relevance across broad applications in electronics, optoelectronics, sensing, and catalysis. Understanding how to manipulate the material growth to achieve the desired properties is the key to tailoring the material towards a specific application. In this work, we investigate the growth of vertically standing MoS_2 nanosheets by chemical vapor deposition on vicinal and on-axis 4H-SiC (0001) substrates. In both cases the MoS_2 flakes exhibit three preferred orientations, aligning with the $\langle 11\bar{2}0 \rangle$ substrate directions due to strain minimization of a MoO_2 intermediate phase.

Whereas MoS_2 grown on vicinal SiC substrates exhibits strict near-vertical alignment, scanning electron microscopy and near-edge X-ray absorption fine structure (NEXAFS) measurements indicate a near-random vertical orientation when MoS_2 is grown on on-axis SiC. Photoemission spectroscopy and NEXAFS measurements indicate the presence of defects and disordered edges which establish the suitability of the material for applications in sensing and catalysis.

1. Introduction

Layered transition metal dichalcogenides (TMDs) such as molybdenum disulfide (MoS_2) have been demonstrated as a versatile material with diverse applications ranging from nano- and optoelectronics [1–3] to catalysis [4] and chemical sensing [5–7]. The performance of devices in these applications is heavily dependent on the MoS_2 layer morphology. For electronics and optoelectronics high performance is achieved by exploiting the transition from an indirect to direct bandgap by isolating monolayer MoS_2, and devices benefit from the lack of dangling bonds on the exposed basal plane [1]. On the other hand, the catalytic activity or chemical sensitivity of the material is enhanced by exposed edges where dangling bonds provide increased chemical activity compared to the inert basal plane [6,8,9]. Consequently, the ability to synthesize densely packed, vertically standing MoS_2 nanosheets will facilitate improved performance of MoS_2 in these areas.

Vertically standing MoS_2 layers can be synthesized by vapor transport methods such as sulfurization of molybdenum layers [6,10–12] or chemical vapor deposition (CVD) [13–17]. The sulfurization approach enables tunability of the film morphology by control of the metal layer thickness. At low thicknesses the MoS_2 layers form with the basal plane parallel to the substrate surface, whereas at high thicknesses a vertically-aligned MoS_2 layer grows with exposed layer edges at the surface [10]. For MoS_2 grown by CVD, the orientation of the MoS_2 layer (vertical or horizontal) depends on the ratio of molybdenum and sulfur precursors in the initial growth stages, with vertical growth favoured when the metal precursor concentration exceeds that of the sulfur precursor [16]. On substrates

such as SiC and sapphire, vertically standing MoS_2 layers further adopt three preferred lateral orientations with respect to the substrate due to the surface symmetry [16,17].

Vicinal (off-axis) substrates are often employed in epitaxial crystal growth and self-assembly of low-dimensional nanostructures on surfaces [18]. The periodic arrangement of atomic steps with densities selected according to the vicinal angle provides a template for the nucleation of adsorbates on the surface. Recently, vicinal surfaces have been shown to be key to achieving the growth of single crystal monolayer hBN [19,20] and MoS_2 [21] at centimetre scales. In these instances, alignment of a particular edge orientation with the step edge, repeated across the sample surface, allows grains to coalesce without grain boundaries. In light of this, the role of the substrate orientation on the growth of vertically aligned MoS_2 layers is of significant interest.

In this work, we demonstrate that the orientation and vertical alignment of MoS_2 nanosheets grown on 4H-SiC (0001) by CVD is influenced by the substrate vicinal angle. On a vicinal substrate the MoS_2 nanosheets exhibit near-perfect vertical alignment, and form with three preferential orientations corresponding to the high-symmetry directions of the SiC(0001) surface. Meanwhile, on the on-axis substrates the sheets are more disordered, and the vertical alignment is not distinct. Our microscopic investigations are supported by synchrotron-based X-ray photoemission spectroscopy (XPS) and near-edge x-ray absorption fine structure (NEXAFS) measurements which additionally reveal the presence of defects and establish the suitability of the material for applications in sensing and catalysis.

2. Experimental Details

2.1 MoS_2 Synthesis

MoS_2 was grown on 4H-SiC(0001) substrates cut on-axis (Cree Inc.) and 4° off-axis towards $\langle 11\bar{2}0 \rangle$ (Norstel) by CVD. Prior to MoS_2 synthesis the substrates were washed under sonication for 15 min

each in acetone, ethanol, and deionized water to remove organic residue. Substrates were then loaded into a horizontal quartz tube furnace 2.5 cm downstream from an alumina crucible containing 30 mg of MoO_3 powder. Another crucible containing 500 mg of sulfur powder was placed in the upstream zone. Before synthesis, the tube was purged with 800 sccm Ar flow for 1 h before reducing to 600 sccm. After annealing the sample at 150 °C for 20 min to remove adsorbed contaminants, MoO_3 was evaporated at 750 °C simultaneously with sulfur at 280 °C under atmospheric pressure. A detailed description and schematics of the growth procedure can be found in the supporting information (SI).

2.2 Material Characterization

The MoS_2/SiC sample morphology was characterized by atomic force microscopy (AFM, NT-MDT Solver), field-emission scanning electron microscopy (Zeiss Sigma FE-SEM) and transmission electron microscopy (TEM, Jeol 2100F). TEM samples were prepared by scratching the MoS_2 flakes from the surface, dispersing in ethanol and drop-casting onto TEM grids. Raman spectra were acquired using a Renishaw inVia Raman spectrometer with a frequency doubled NdYAG laser (λ = 532 nm). The laser was focused using a 50× objective lens giving a spot size of approximately 1 μm, and a laser power of < 5 mW. Atomic force microscopy (AFM) images were acquired with an NT-MDT scanning probe microscope in tapping mode using Si cantilevers (NSG30, NT-MDT), and a Bruker Dimension ICON AFM system operated in tapping and contact modes using Si cantilevers (ScanAsyst-Air, Bruker). AFM images were processed using the Gwyddion software package [22]. Synchrotron-based XPS and near-edge X-ray absorption fine structure (NEXAFS) measurements were acquired at the soft X-ray Spectroscopy beamline of the Australian Synchrotron. The synchrotron-based XPS spectra were acquired with a photon energy of 350 eV for C 1s, Mo 3d, S 2p and Si 2p core level spectra, and 650 eV for O 1s, in order to enhance the surface sensitivity and photoionization cross-sections. The spectra were measured at a pass energy of 10 eV for an overall energy resolution of 0.29 eV. Binding

energies were calibrated using a sputtered gold foil in electrical contact with the sample stage. XPS spectra were analysed using CasaXPS [23]. NEXAFS spectra were acquired using linearly polarized light at three angles of incidence with respect to the sample surface plane: glancing incidence (θ = 20°), tilt-independent "magic" angle (θ = 55°), and normal incidence (θ = 90°). The signal measured is the total electron yield and is recorded by measuring the drain current from the samples. Bulk MoS_2 reference spectra were simultaneously acquired for calibration of the photon energies, and the photon flux was measured by collecting the current from a gold mesh placed in the bath of the beam. NEXAFS spectra were normalised using the QANT software package [24], and all spectra were normalised against the incoming photon flux determined by the current measured from a gold mesh in the path of the beam.

3. Results and Discussion

3.1 MoS_2/SiC Characterization

SEM images of the CVD-grown MoS_2 are shown in Figure 1 (a) and (b) for the off-axis and on-axis SiC substrates, respectively. In both cases, the MoS_2 grows with a predominantly vertical orientation similar to previous observations [15,16], with only a small number of flat-lying crystals. On the off-axis substrate in (a), the vertical flakes appear almost perfectly upright, whereas on the on-axis substrate in (b) the flakes appear to be tilted, with some flat-lying crystals. On both substrates the flakes exhibit three distinct lateral orientations as shown by the histograms in Figure 1 (c) and (d), although there is more variation in the orientation of MoS_2 on the on-axis substrate. Based on the known orientation of the substrate we can determine that the flakes grow in three preferred orientations along $[11\bar{2}0]$, $[1\bar{2}10]$ and $[2\bar{1}10]$ lattice directions of the SiC substrate. The crystal model for these orientations is shown in Figure 1 (e) and (f).

AFM measurements were taken in order to ascertain the height of the MoS_2 flakes. Figure 2(a) shows a topographic AFM image of vertical MoS_2 flakes grown on an off-axis 4H-SiC sample with a lower density. As was observed by SEM, three distinct lateral orientations are also seen in the AFM image. A line profile taken along the white dotted line is shown in Figure 2(b). The height of the flake measured from the line profile is 1.3 μm. Thickness of the flake measured from the AFM line profile (approximately 1.5 μm) is unreliable due to the interaction of the AFM tip apex with the surface which exaggerates the thickness measurement. The true MoS_2 flake thickness was measured by TEM. Figure 2(d) shows a TEM image of the MoS_2 nanosheets, and the selected area electron diffraction (SAED) pattern inset confirms the presence of two MoS_2 crystals with different orientations viewed along the [0001] zone axis. When viewed along the edge of the flake, as shown in Figure 2(e), the thickness of the MoS_2 flakes was found to be approximately 40 nm or 60 layers of MoS_2.

The Raman spectrum of the MoS_2 nanosheets is shown in Figure 2(c). Peaks at 384 cm^{-1} and 409 cm^{-1} correspond to the in-plane E^1_{2g} and out-of-plane A_{1g} of the S–Mo–S sandwiched structure in 2H-MoS_2 [25,26]. The peak separation of 25 cm^{-1} is consistent with the observed peak separation for bulk MoS_2,[25,26] as expected for the 40 nm thick crystals. Notably, the high intensity ratio between the A_{1g} and E^1_{2g} peaks has been previously associated with the high density of exposed edges in vertically standing MoS_2 nanosheets [10,11,14,15].

The chemical composition of the MoS_2 flakes was determined by synchrotron-based XPS and the deconvolution of the spectra are shown in Figure 3 and Tables S1 and S2 (Supporting Information). Figure 3 shows the Mo 3d (a) and S 2p (b) core level spectra of the on- and off-axis samples. In the Mo 3d core level, an intense, narrow doublet at 229.7 eV and 232.9 eV arises from MoS_2, with the corresponding S 2s component visible at 226.8 eV [27]. A higher binding energy component at 233.0 eV and 236.1 eV can be attributed to the Mo^{6+} chemical state indicating a small amount of residual MoO_3 [27]. In both cases the residual MoO_3 accounts for < 1.6 % of the total spectral intensity. A low

binding energy doublet is also observed at 229.4 eV and 232.5 eV which we attribute to defects in MoS_2. These contributions also appear in the S 2p core level spectrum shifted by -0.3 – -0.4 eV from the MoS_2 peak position. The ratio of defective to pristine MoS_2 is 0.05 ± 0.01 for the sample grown on vicinal SiC and 0.15 ± 0.02 for the sample grown on on-axis SiC, suggesting higher quality growth on the vicinal substrate. The defect-related sulfur component was not included in the S 2s region due to the small photoionization cross-section of S 2p photoelectrons compared to Mo 3d. On both substrates, considering the spectral weight of the Mo 3d defect-related component, the corresponding S 2s contribution would be expected to give less than 1 % of the overall spectral intensity. Similar XPS observations of defects related to sulfur deficiencies have been made in WS_2 [28] and in MoS_2 [29,30]. Taking into account the photoionization cross-section of the Mo 3d and S 2s core levels, the peak areas give an atomic S:Mo ratio of 1.89 ± 0.10 indicating a slightly sub-stoichiometric MoS_2 layer. The S:Mo ratio was calculated to be 1.91 ± 0.08 using data from a laboratory XPS system which verifies that the value is not an artefact arising due to the textured surface. The S:Mo ratio is consistent with the assignment of the additional core level peaks as defects associated with a sulfur deficiency. The shift in the core level binding energies arises due to band bending in highly defective MoS_2 regions [30]. Although passivation of sulfur vacancies with other atomic species is a possibility [31], we do not believe that to be the case here. Given the growth environment the element mostly likely to passivate defects would be oxygen, however incorporation of oxygen into a MoO_xS_y compound would result in a shift of the Mo 3d and S 2p electrons to higher binding energies [32,33].

To gain further insight into the electronic structures we performed NEXAFS spectroscopy to probe the empty electronic states of the system and their geometry. Figure 4(a) shows a typical sulfur K-edge NEXAFS spectrum measured for MoS_2 grown on SiC. The experimental data are shown as black dots, and the synthetic fit to the data given by the coloured peaks is indicated by the red line. The main absorption peak is made up of two components at 2471.5 eV and 2471.7 eV that cannot be individually resolved and is produced by transitions of S 1s core level electrons into S 3p states

hybridized with Mo 4d states (purple peak). A shoulder at 2473.2 eV is a dipole-forbidden S 1s to 4d transition (green peak), however it is still observed with reduced intensity due to hybridization with Mo 5p states [8,34]. There is a pre-edge feature that appears at approximately 2466 eV in the off-axis sample and 2464 eV in the on-axis sample (see Figure 4(b) and (c)). Pre-edge features have previously been calculated and observed experimentally and associated with corrugated edges in exfoliated MoS_2 crystals [8]. Irregularities at the edges of the crystal result in localization of S 3p–Mo 4d states and give rise to pre-edge absorption. Similarly, the pre-edge features observed here may also be caused by exposed edges in the vertically standing flakes. The fact that they are only observed at normal incidence may be due to increased interaction of the incident X-rays with the edges of the flakes, compared to off-normal measurement angles where there is more interaction with the basal planes. The sulfur K post-edge structure is made up of transitions into p-like states at photon energies between 2480 and 2485 eV [8,34–36]. The post-edge features in this work are fit empirically (Figure 4(a)) without any consideration of the physical transitions. This is due to some artefacts that remain after normalization against the incoming photon flux. Further details are provided in the Supporting Information (Figure S3).

NEXAFS spectroscopy can provide insight in the geometry of the MoS_2 nanosheets by measuring the intensity variation of particular spectral features at different X-ray incidence angles. On a surface with three-fold symmetry, in the case of 100% linearly polarized light (typical for an undulator beamline), the intensity variation of features associated with transitions into states with vector-type orbitals varies as

$$I(\alpha,\theta) \propto 1 + \frac{1}{2}(3\cos^2\theta - 1)(3\cos^2\alpha - 1) \quad (1)$$

where θ is the X-ray angle of incidence with respect to the sample surface, and α is the tilt angle of the orbital with respect to the surface normal [37].

The sulfur K-edge NEXAFS spectra were measured at three incident angles: glancing incidence (20°), normal incidence (90°) and the tilt-independent “magic angle” (55°). The spectra from the off-axis

substrate, shown in Figure 4(b), exhibits distinct variations in the primary absorption peak intensity, whereas the spectra in (c) for the on-axis substrate show only a small intensity variation. The sulfur K-edge peak model from Figure 4(a) was propagated through all spectra to extract the intensity of S 1s → S 3p transition, and the angular variations are shown in the insets of Figure 4(b) and (c). Fitting these values with equation (1) allows average orbital tilt angles of 63.2±0.3° and 56±1°, with respect to the surface normal, to be extracted for the off-axis and on-axis samples, respectively. The calculated orbital tilt angle for the on-axis sample is very close the so-called "magic angle" of 54.7° where, if the excited orbital adopts this geometry, the intensity of the NEXAFS peak will show no dependence on the sample tilt with respect to the incoming beam [37,38]. An alternative interpretation is that there is no preferred orientation of the MoS_2 crystals with uniformly distributed tilt angles. Based on the SEM images (Figure 1(b)) which show that the flakes do not adopt a uniform tilt angle with respect to the surface, the latter interpretation is more appropriate. This also provides a clearer interpretation of the morphology observed in SEM where it is not immediately clear whether the structures observed are tilted, or if they are basal plane-aligned crystals. If the MoS_2 basal plane was aligned with sample surface, we would expect to see a preferred tilt angle complementary to the tilt observed for vertically standing flakes. In contrast to the on-axis substrate, the spectra acquired from MoS_2 grown on the off-axis substrate produce an average orbital tilt angle of 63.2±0.3°, with respect to the surface normal, indicating a strong preferred alignment of the MoS_2 flakes which is also clear in the SEM image (Figure 1(a)).

3.2 Growth Mechanism

During the process of optimizing the growth parameters, some samples were found to contain residual MoO_2 caused by insufficient sulfur supply. This can be seen in the Raman spectrum in Figure 5(a) which contains four additional peaks to the MoS_2 A_{1g} and E^1_{2g} Raman modes. Features at 345 cm^{-1}, 349 cm^{-1}, 363 cm^{-1}, 496 cm^{-1}, and 568 cm^{-1} are attributed to monoclinic MoO_2 [16,39]. By TEM

investigations, we observed flakes which contain both MoS_2 layers and MoO_2 as can be seen in Figure 5(b) and (c). In the image shown in Figure 5(b), MoS_2 can be identified from the fringes on the top left edge of the flake. The plane spacing of 0.65 nm is consistent with the interlayer spacing of MoS_2. In the high-resolution image shown in Figure 5(c), the atomic spacing (0.25 nm) of the inner lattice is consistent with the Mo atom spacing in monoclinic MoO_2 projected along the [010] zone axis. Similarly to the image in (b), fringes at the surface have a layer spacing of 0.65 nm corresponding to the layer spacing of MoS_2.

The growth mechanism of vertically aligned MoS_2 nanosheets was previously elucidated by Vilá et al [16]. At low MoO_3:S ratios the presence of both precursors on the surface result in Frank–van der Merwe (layer-by-layer) MoS_2 growth. Conversely, at high MoO_3:S ratios MoS_2 growth is preceded by Volmer-Weber growth of MoO_2 fins which form due to the excess of the molybdenum precursor on the surface, followed by sulfurization into MoS_2. In the TEM image in Figure 5(b) we observed that the number of layers of MoS_2 is greater at the base of the flake, where it was detached from the SiC substrate, than towards the tip of the triangle. This suggests that sulfurization occurs via diffusion of sulfur from the interface between the substrate surface and the flake [16].

MoS_2 flakes were observed to grow along the $\langle 11\bar{2}0 \rangle$ directions of the SiC substrate consistent with previous reports [16]. This at first seems counter intuitive since the $(11\bar{2}0)$ lattice plane spacing is 1.5426 Å, which is approximately one-quarter of the (002) plane spacing of MoS_2 (6.1475 Å), with a mismatch of 0.37 %. By comparison, the $(1\bar{1}00)$ interplanar distance is 2.6678 Å which is approximately half of the MoS_2 (002) plane spacing, with a much higher mismatch of 15 %. Therefore, one might expect the MoS_2 flakes to be aligned along the $\langle 1\bar{1}00 \rangle$ directions so that the (002) plane of MoS_2 is aligned with the $(11\bar{2}0)$ plane of the SiC substrate in order to minimize strain. Instead, the observed orientation is due to strain minimization between the SiC substrate and the MoO_2 nucleus prior to MoS_2 formation [16].

The MoS_2 flakes exhibit a clear vertical alignment when grown on the off-axis substrate, but the tilt angle is less distinct on the on-axis substrate. The reason for this is not clear based on the experimental data. One difference between the substrate surfaces lies in the step density, which is higher on the off-axis substrate [40], as demonstrated by the surface analysis in Figure S5 (Supporting Information). Considering this, we propose that the change in morphology is due to interaction of MoO_x and S adsorbates with step edges on the surface. Step edges present a diffusion barrier to adatoms on the surface and, as such, the high step density on the vicinal substrate results in a higher probability of forming a MoO_2 critical nucleus in the early growth stages to initiate vertical MoS_2 growth. In contrast, on the on-axis substrate, the lower step density may prevent formation of a MoO_2 critical nucleus while the sulfur concentration at the surface is sufficiently low, therefore affecting the vertical MoS_2 growth. While the high step density on the vicinal surface clearly influences the vertical and lateral flake alignment, we note that epitaxy with the SiC surface still dictates the overall orientation of the flakes. If the step orientation were to play a dominant role, we would expect to see the majority of MoS_2 flakes with the same orientation due to the reduced symmetry of the vicinal surface, as has been recently demonstrated for h-BN grown on vicinal Cu(110) [19,20]. Alternatively, the existence of three MoS_2 orientations on the surface may be indicative that the surface of the vicinal substrate initially possess jagged step edges, as opposed to parallel, singly oriented steps, or the growth process induces jaggedness in the steps [41]. We note that the precise morphology of the 4H-SiC surfaces could not be verified by AFM, although the increased step density of the vicinal surface compared to the on-axis surface is evident in Figure S5 (Supporting Information). It is noted that a single vicinal angle and orientation was used in this study. Exploration of the influence of other vicinal angles and orientations on the MoS_2 flake orientation is subject to further investigation.

4 Conclusion

The lateral orientation and vertical alignment of MoS_2 nanosheets grown by CVD has been demonstrated to be influenced by the vicinal angle of the underlying 4H-SiC(0001) substrate. Employing an off-axis substrate enables strict vertical alignment of the MoS_2 nanosheets and near-perfect alignment along the $\langle 11\bar{2}0 \rangle$ SiC lattice directions. On the on-axis substrates, under identical growth conditions, both the vertical alignment and lateral orientations are less distinct, though the lateral orientation is still predominately determined by the surface symmetry. The strict vertical alignment of MoS_2 was confirmed from the angular dependence of the S 1s → S 3p transition in the NEXAFS spectra. Synchrotron-based XPS measurements, along with NEXAFS spectroscopy, indicate the presence of defects which suggests that the material would be suitable for applications in catalysis and sensing.

Acknowledgements

The data reported in this paper were obtained at the Central Analytical Research Facility (CARF) operated by QUT's Institute for Future Environments. The contributions of Dr Jamie Riches in the TEM analysis is kindly acknowledged. This research was undertaken on the SXR beamline at the Australian Synchrotron, part of ANSTO. J.B. acknowledges the support from the Australian Government Research Training Program. M.S. acknowledges funding from Australian Research Council (ARC) - Discovery Project, DP150101939. N.M. acknowledges funding from the ARC – Discovery Project, DP200102546. D.Q. acknowledges the support of the Australian Research Council (Grant No. FT160100207).

References

[1] Q.H. Wang, K. Kalantar-Zadeh, A. Kis, J.N. Coleman, M.S. Strano, Electronics and optoelectronics of two-dimensional transition metal dichalcogenides, Nat. Nanotechnol. 7

(2012) 699. https://doi.org/10.1038/nnano.2012.193.

[2] M. Chhowalla, D. Jena, H. Zhang, Two-dimensional semiconductors for transistors, Nat. Rev. Mater. 1 (2016) 16052. https://doi.org/10.1038/natrevmats.2016.52.

[3] W. Zhang, Q. Wang, Y. Chen, Z. Wang, A.T.S. Wee, Van der Waals stacked 2D layered materials for optoelectronics, 2D Mater. 3 (2016) 022001. https://doi.org/10.1088/2053-1583/3/2/022001.

[4] X. Chia, A.Y.S. Eng, A. Ambrosi, S.M. Tan, M. Pumera, Electrochemistry of Nanostructured Layered Transition-Metal Dichalcogenides, Chem. Rev. 115 (2015) 11941–11966. https://doi.org/10.1021/acs.chemrev.5b00287.

[5] C. Anichini, W. Czepa, D. Pakulski, A. Aliprandi, A. Ciesielski, P. Samorì, Chemical sensing with 2D materials, Chem. Soc. Rev. 47 (2018) 4860–4908. https://doi.org/10.1039/C8CS00417J.

[6] S.-Y. Cho, S.J. Kim, Y. Lee, J.-S. Kim, W.-B. Jung, H.-W. Yoo, J. Kim, H.-T. Jung, Highly Enhanced Gas Adsorption Properties in Vertically Aligned MoS_2 Layers, ACS Nano. 9 (2015) 9314–9321. https://doi.org/10.1021/acsnano.5b04504.

[7] M. Shafiei, J. Bradford, H. Khan, C. Piloto, W. Wlodarski, Y. Li, N. Motta, Low-operating temperature NO2 gas sensors based on hybrid two-dimensional SnS_2-reduced graphene oxide, Appl. Surf. Sci. 462 (2018) 330–336. https://doi.org/10.1016/j.apsusc.2018.08.115.

[8] A. Parija, Y.H. Choi, Z. Liu, J.L. Andrews, L.R. De Jesus, S.C. Fakra, M. Al-Hashimi, J.D. Batteas, D. Prendergast, S. Banerjee, Mapping Catalytically Relevant Edge Electronic States of MoS_2, ACS Cent. Sci. 4 (2018) 493–503. https://doi.org/10.1021/acscentsci.8b00042.

[9] J. Kibsgaard, Z. Chen, B.N. Reinecke, T.F. Jaramillo, Engineering the surface structure of MoS_2 to preferentially expose active edge sites for electrocatalysis, Nat. Mater. 11 (2012) 963–969. https://doi.org/10.1038/nmat3439.

[10] Y. Jung, J. Shen, Y. Liu, J.M. Woods, Y. Sun, J.J. Cha, Metal Seed Layer Thickness-Induced Transition From Vertical to Horizontal Growth of MoS_2 and WS_2, Nano Lett. 14 (2014) 6842–6849. https://doi.org/10.1021/nl502570f.

[11] D. Kong, H. Wang, J.J. Cha, M. Pasta, K.J. Koski, J. Yao, Y. Cui, Synthesis of MoS_2 and $MoSe_2$ Films with Vertically Aligned Layers, Nano Lett. 13 (2013) 1341–1347. https://doi.org/10.1021/nl400258t.

[12] G. Deokar, N.S. Rajput, J. Li, F.L. Deepak, W. Ou-Yang, N. Reckinger, C. Bittencourt, J.-F. Colomer, M. Jouiad, Toward the use of CVD-grown MoS_2 nanosheets as field-emission source, Beilstein J. Nanotechnol. 9 (2018) 1686–1694. https://doi.org/10.3762/bjnano.9.160.

[13] G.R. Bhimanapati, T. Hankins, Y. Lei, R.A. Vilá, I. Fuller, M. Terrones, J.A. Robinson, Growth and Tunable Surface Wettability of Vertical MoS_2 Layers for Improved Hydrogen Evolution Reactions, ACS Appl. Mater. Interfaces. 8 (2016) 22190–22195. https://doi.org/10.1021/acsami.6b05848.

[14] H. Li, H. Wu, S. Yuan, H. Qian, Synthesis and characterization of vertically standing MoS_2 nanosheets, Sci. Rep. 6 (2016) 21171. https://doi.org/10.1038/srep21171.

[15] F. Lan, Z. Lai, Y. Xu, H. Cheng, Z. Wang, C. Qi, J. Chen, S. Zhang, Synthesis of Vertically Standing MoS_2 Triangles on SiC, Sci. Rep. 6 (2016) 31980. https://doi.org/10.1038/srep31980.

[16] R.A. Vilá, K. Momeni, Q. Wang, B.M. Bersch, N. Lu, M.J. Kim, L.Q. Chen, J.A. Robinson, Bottom-up synthesis of vertically oriented two-dimensional materials, 2D Mater. 3 (2016) 041003. https://doi.org/10.1088/2053-1583/3/4/041003.

[17] D. Dumcenco, D. Ovchinnikov, O. Lopez Sanchez, P. Gillet, D.T.L. Alexander, S. Lazar, A. Radenovic, A. Kis, Large-area MoS_2 grown using H_2S as the sulphur source, 2D Mater. 2 (2015) 044005. https://doi.org/10.1088/2053-1583/2/4/044005.

[18] C. Tegenkamp, Vicinal surfaces for functional nanostructures, J. Phys. Condens. Matter. 21

(2008) 13002. https://doi.org/10.1088/0953-8984/21/1/013002.

[19] K. V Bets, N. Gupta, B.I. Yakobson, How the Complementarity at Vicinal Steps Enables Growth of 2D Monocrystals, Nano Lett. 19 (2019) 2027–2031. https://doi.org/10.1021/acs.nanolett.9b00136.

[20] L. Wang, X. Xu, L. Zhang, R. Qiao, M. Wu, Z. Wang, S. Zhang, J. Liang, Z. Zhang, Z. Zhang, W. Chen, X. Xie, J. Zong, Y. Shan, Y. Guo, M. Willinger, H. Wu, Q. Li, W. Wang, P. Gao, S. Wu, Y. Zhang, Y. Jiang, D. Yu, E. Wang, X. Bai, Z.-J. Wang, F. Ding, K. Liu, Epitaxial growth of a 100-square-centimetre single-crystal hexagonal boron nitride monolayer on copper, Nature. 570 (2019) 91–95. https://doi.org/10.1038/s41586-019-1226-z.

[21] P. Yang, S. Zhang, S. Pan, B. Tang, Y. Liang, X. Zhao, Z. Zhang, J. Shi, Y. Huan, Y. Shi, S.J. Pennycook, Z. Ren, G. Zhang, Q. Chen, X. Zou, Z. Liu, Y. Zhang, Epitaxial Growth of Centimeter-Scale Single-Crystal MoS_2 Monolayer on Au(111), ACS Nano. 14 (2020) 5036–5045. https://doi.org/10.1021/acsnano.0c01478.

[22] D. Nečas, P. Klapetek, Gwyddion: An open-source software for SPM data analysis, Cent. Eur. J. Phys. 10 (2012) 181–188. https://doi.org/10.2478/s11534-011-0096-2.

[23] CasaXPS version 2.3.1PR1.0, (1999).

[24] E. Gann, C.R. McNeill, A. Tadich, B.C.C. Cowie, L. Thomsen, Quick AS NEXAFS Tool (QANT): a program for NEXAFS loading and analysis developed at the Australian Synchrotron, J. Synchrotron Radiat. 23 (2016) 374–380. https://doi.org/doi:10.1107/S1600577515018688.

[25] C. Lee, H. Yan, L.E. Brus, T.F. Heinz, J. Hone, S. Ryu, Anomalous Lattice Vibrations of Single- and Few-Layer MoS_2, ACS Nano. 4 (2010) 2695–2700. https://doi.org/10.1021/nn1003937.

[26] H. Li, Q. Zhang, C.C.R. Yap, B.K. Tay, T.H.T. Edwin, A. Olivier, D. Baillargeat, From Bulk to Monolayer MoS_2: Evolution of Raman Scattering, Adv. Funct. Mater. 22 (2012) 1385–1390. https://doi.org/10.1002/adfm.201102111.

[27] D. Ganta, S. Sinha, R.T. Haasch, 2-D Material Molybdenum Disulfide Analyzed by XPS, Surf. Sci. Spectra. 21 (2014) 19–27. https://doi.org/10.1116/11.20140401.

[28] C. Kastl, R.J. Koch, C.T. Chen, J. Eichhorn, S. Ulstrup, A. Bostwick, C. Jozwiak, T.R. Kuykendall, N.J. Borys, F.M. Toma, S. Aloni, A. Weber-Bargioni, E. Rotenberg, A.M. Schwartzberg, Effects of Defects on Band Structure and Excitons in WS_2 Revealed by Nanoscale Photoemission Spectroscopy, ACS Nano. 13 (2019) 1284–1291. https://doi.org/10.1021/acsnano.8b06574.

[29] D. Pierucci, H. Henck, Z. Ben Aziza, C.H. Naylor, A. Balan, J.E. Rault, M.G. Silly, Y.J. Dappe, F. Bertran, P. Le Fèvre, F. Sirotti, A.T.C. Johnson, A. Ouerghi, Tunable Doping in Hydrogenated Single Layered Molybdenum Disulfide, ACS Nano. 11 (2017) 1755–1761. https://doi.org/10.1021/acsnano.6b07661.

[30] M. Donarelli, F. Bisti, F. Perrozzi, L. Ottaviano, Tunable sulfur desorption in exfoliated MoS_2 by means of thermal annealing in ultra-high vacuum, Chem. Phys. Lett. 588 (2013) 198–202. https://doi.org/10.1016/j.cplett.2013.10.034.

[31] S. Barja, S. Refaely-Abramson, B. Schuler, D.Y. Qiu, A. Pulkin, S. Wickenburg, H. Ryu, M.M. Ugeda, C. Kastl, C. Chen, C. Hwang, A. Schwartzberg, S. Aloni, S.-K. Mo, D. Frank Ogletree, M.F. Crommie, O. V Yazyev, S.G. Louie, J.B. Neaton, A. Weber-Bargioni, Identifying substitutional oxygen as a prolific point defect in monolayer transition metal dichalcogenides, Nat. Commun. 10 (2019) 3382. https://doi.org/10.1038/s41467-019-11342-2.

[32] J.. Dupin, D. Gonbeau, I. Martin-Litas, P. Vinatier, A. Levasseur, Amorphous oxysulfide thin films MO_yS_z (M=W, Mo, Ti) XPS characterization: structural and electronic pecularities, Appl. Surf. Sci. 173 (2001) 140–150. https://doi.org/10.1016/S0169-4332(00)00893-X.

[33] J. Bradford, M. Shafiei, J. MacLeod, N. Motta, Synthesis and characterization of WS_2/graphene/SiC van der Waals heterostructures via WO_{3-x} thin film sulfurization, Sci. Rep. 10 (2020) 17334. https://doi.org/10.1038/s41598-020-74024-w.

[34] D. Li, G.M. Bancroft, M. Kasrai, M.E. Fleet, X.H. Feng, K.H. Tan, Polarized X-ray absorption spectra and electronic structure of molybdenite (2H-MoS2), Phys. Chem. Miner. 22 (1995) 123–128. https://doi.org/10.1007/BF00202472.

[35] M. Dadsetani, H. Nejatipour, T. Nouri, First-principles study of the sulfur K and L2,3 edges of transition metal disulfide monolayers, MS2 (M=Mo, W and Re), Phys. E Low-Dimensional Syst. Nanostructures. 73 (2015) 198–206. https://doi.org/10.1016/j.physe.2015.05.025.

[36] L. Cai, J. He, Q. Liu, T. Yao, L. Chen, W. Yan, F. Hu, Y. Jiang, Y. Zhao, T. Hu, Z. Sun, S. Wei, Vacancy-Induced Ferromagnetism of MoS_2 Nanosheets, J. Am. Chem. Soc. 137 (2015) 2622–2627. https://doi.org/10.1021/ja5120908.

[37] J. Stöhr, NEXAFS Spectroscopy, Springer Science & Business Media, 2013.

[38] G. Hähner, Near edge X-ray absorption fine structure spectroscopy as a tool to probe electronic and structural properties of thin organic films and liquids, Chem. Soc. Rev. 35 (2006) 1244–1255. https://doi.org/10.1039/B509853J.

[39] M.A. Camacho-López, L. Escobar-Alarcón, M. Picquart, R. Arroyo, G. Córdoba, E. Haro-Poniatowski, Micro-Raman study of the m-MoO_2 to α-MoO_3 transformation induced by cw-laser irradiation, Opt. Mater. (Amst). 33 (2011) 480–484. https://doi.org/10.1016/j.optmat.2010.10.028.

[40] H. Nakagawa, S. Tanaka, I. Suemune, Self-Ordering of Nanofacets on Vicinal SiC Surfaces, Phys. Rev. Lett. 91 (2003) 226107. https://doi.org/10.1103/PhysRevLett.91.226107.

[41] C. D. Frye, C. K. Saw, B. Padavala, N. Khan, R. J. Nikolic, J. H. Edgar, Suppression of Rotational Twins in Epitaxial $B_{12}P_2$ on 4H-SiC, Cryst. Growth & Des. 18 (2017) 669–676. https://doi.org/10.1021/acs.cgd.7b00867.

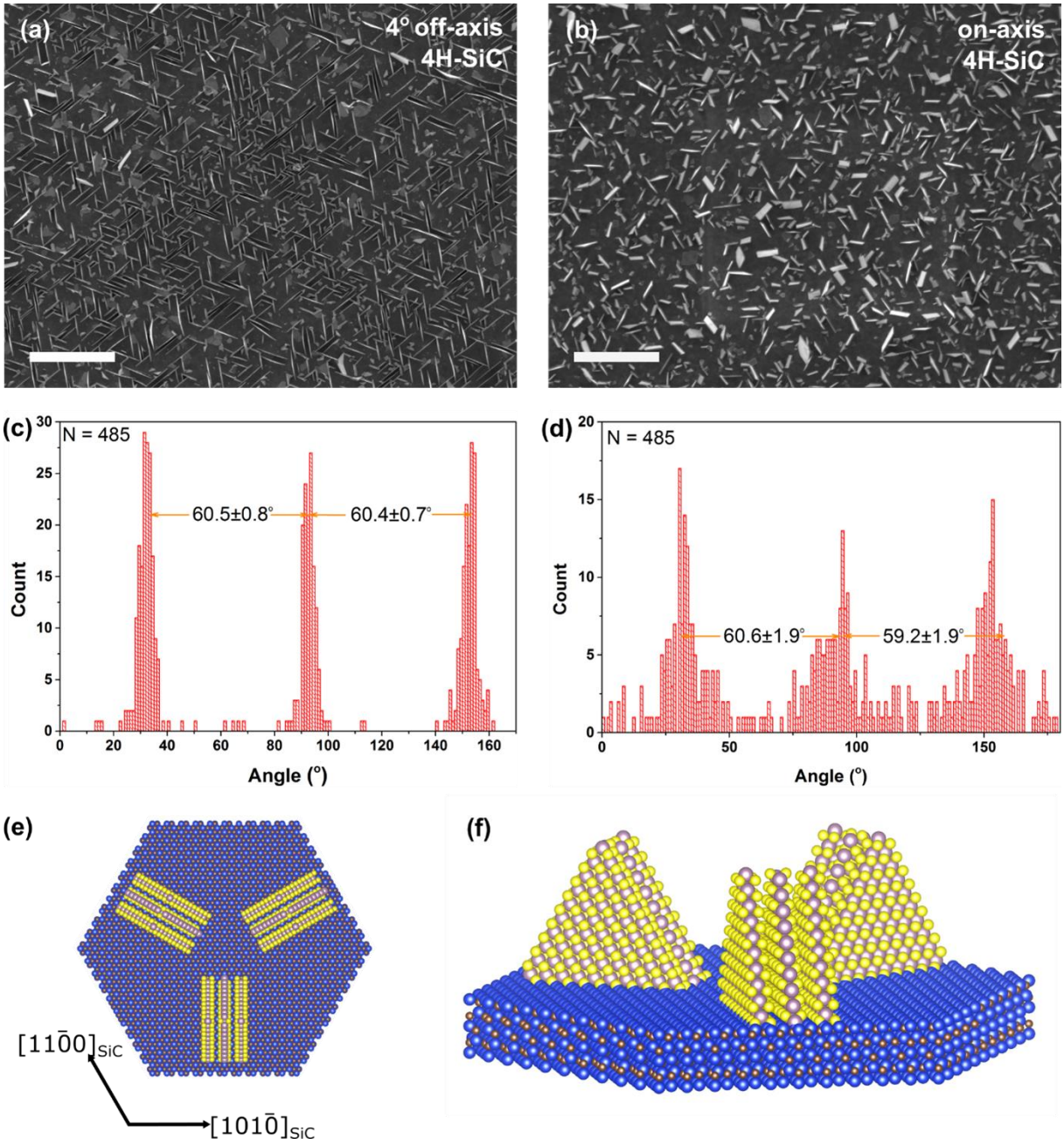

Figure 1: (a) and (b) SEM images of MoS_2 nanosheets grown on 4° off-axis, and on-axis 4H-SiC, respectively. The scale bars in (a) and (b) are 10 μm and 5 μm, respectively. The corresponding distributions of the flake orientations are shown in (c) and (d). Angles are measured with respect to the image horizontal, and are shifted to lie in a 0-180° range; (e) and (f) Crystal model: top view and side view of the oriented, vertically MoS_2 nanosheets on 4H-SiC. The blue, brown, purple and yellow spheres represent silicon, carbon, molybdenum, and sulfur atoms, respectively.

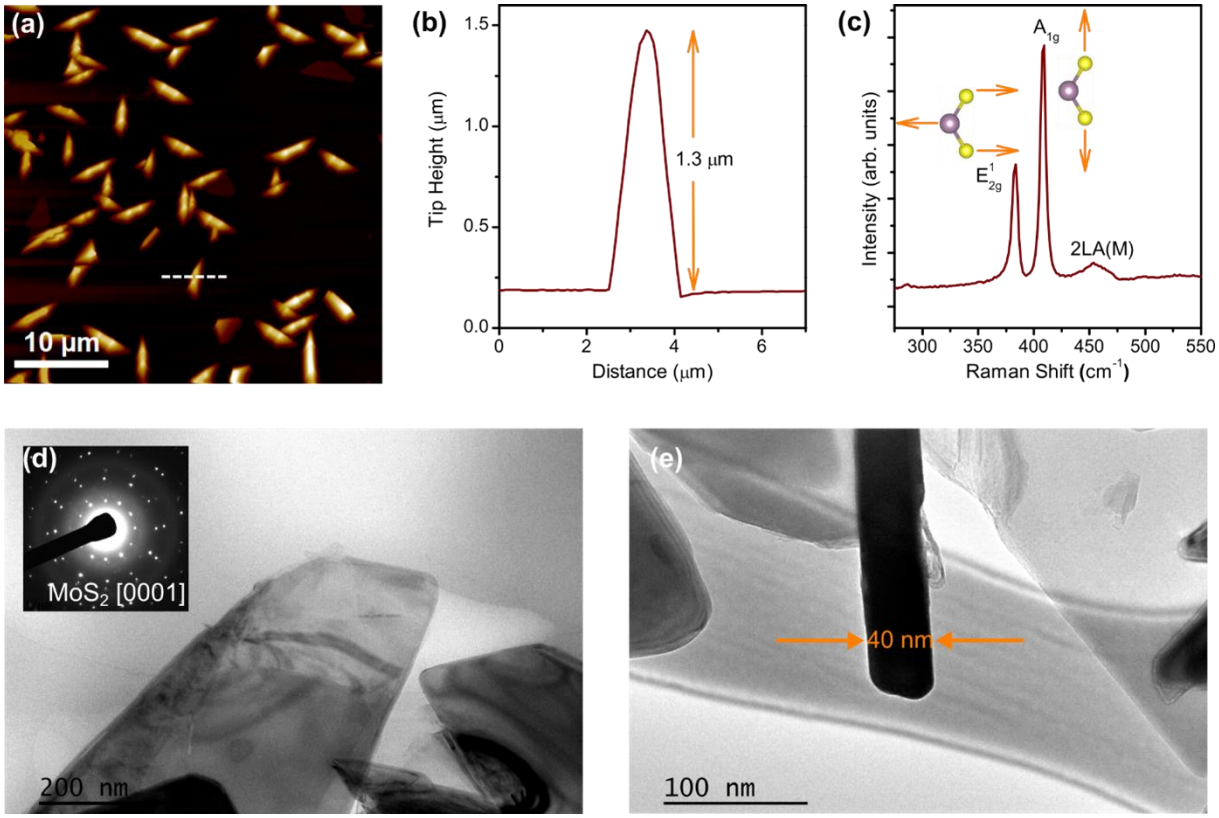

Figure 2: (a) AFM topography image of vertical MoS_2 on SiC; (b) AFM tip height profile taken along the white dotted line in (b); (c) Raman spectrum of the vertical MoS_2 flakes; (d) TEM image of MoS_2 flakes viewed along the MoS_2 [0001] zone axis (inset: SAED pattern); and (e) TEM image of the MoS_2 flake edge.

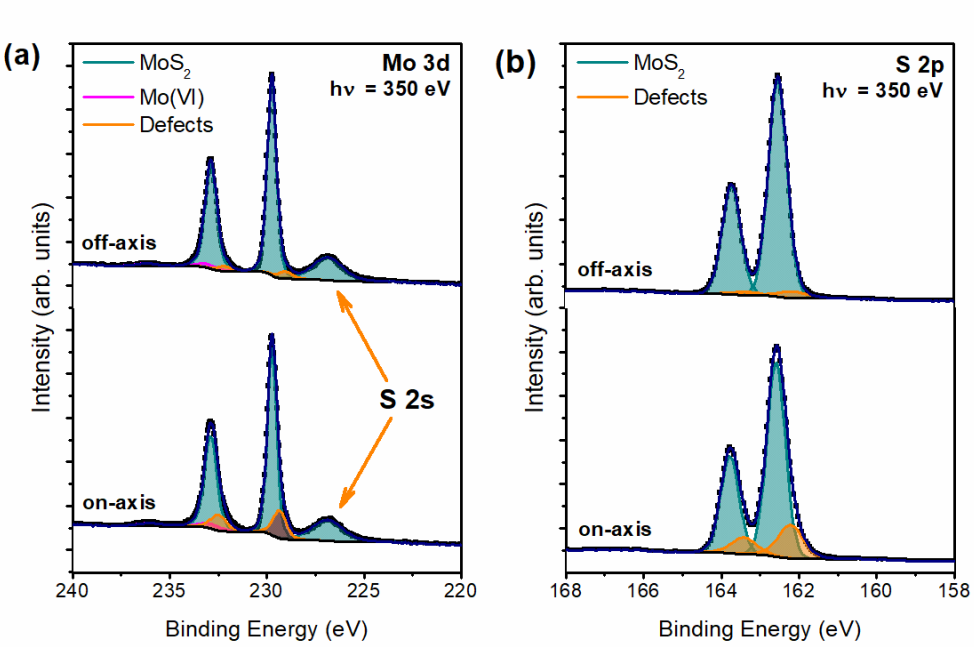

Figure 3: Synchrotron-based XPS analysis. High resolution Mo 3d (a) and S 2p (b) core level spectra for MoS_2 nanosheets.

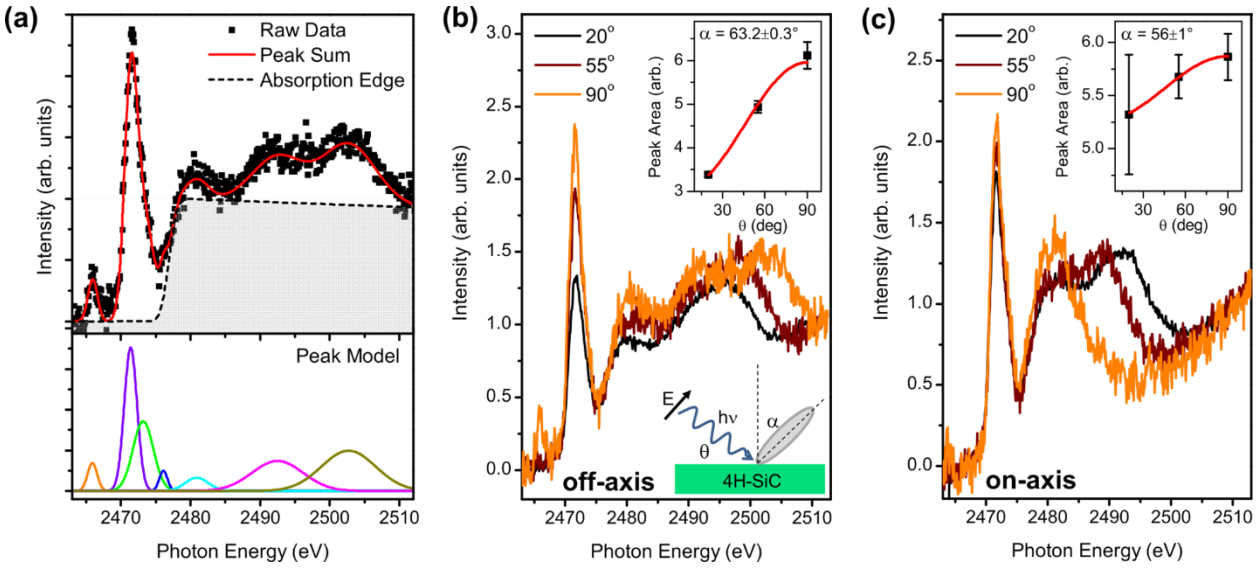

Figure 4: (a) Representative synthetic fit to the sulfur K-edge NEXAFS spectrum for MoS_2 flakes grown on SiC. (b) and (c) Angular dependence of the sulfur K-edge NEXAFS spectra for MoS_2 nanosheets grown on (b) off-axis and (c) on-axis SiC substrates. The X-ray angle of incidence is measured with respect to the sample surface as shown schematically in (a). Intensity variations for the S 1s → S 3p transition (purple peak) are shown in the insets of (b) and (c) with fits to equation (1).

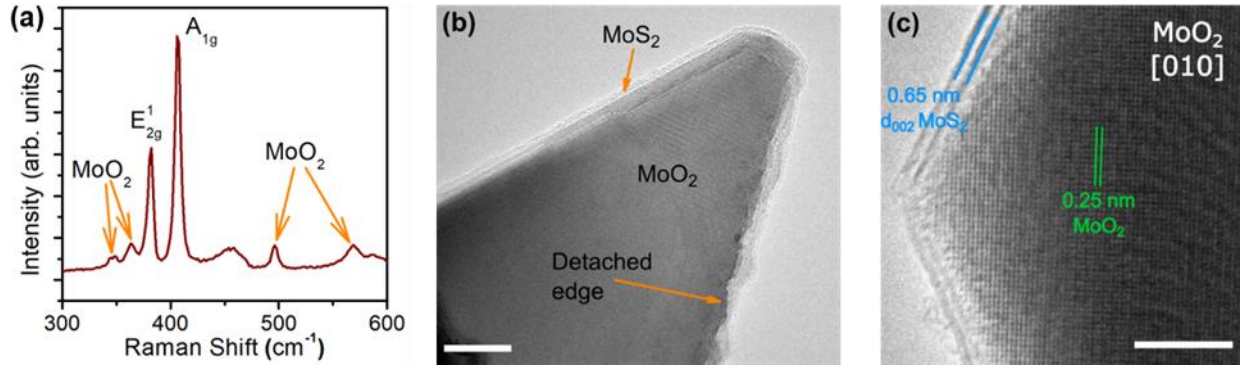

Figure 5: (a) Raman spectrum of an incompletely sulfurized MoS_2 fin; (b) TEM image of an incompletely sulfurized MoS_2 (scale bar is 20 nm); and (c) HRTEM image showing the MoO_2 lattice and MoS_2 layers.